
Vehicle Dynamics in Non-Collinear Low-Velocity, Rear End Collisions

Herbert M. Guzman and Whitman E. McConnell
Biodynamic Research Corporation

Darrin A. Smith
Injury Sciences Corporation

Reprinted From: **Accident Reconstruction 2004**
(SP-1873)

ISBN 0 7680 1427-1



9 780768 014273

SAE *International*[™]

2004 SAE World Congress
Detroit, Michigan
March 8-11, 2004

All rights reserved. No part of this publication may be reproduced, stored in a retrieval system, or transmitted, in any form or by any means, electronic, mechanical, photocopying, recording, or otherwise, without the prior written permission of SAE.

For permission and licensing requests contact:

SAE Permissions
400 Commonwealth Drive
Warrendale, PA 15096-0001-USA
Email: permissions@sae.org
Fax: 724-772-4891
Tel: 724-772-4028



For multiple print copies contact:

SAE Customer Service
Tel: 877-606-7323 (inside USA and Canada)
Tel: 724-776-4970 (outside USA)
Fax: 724-776-1615
Email: CustomerService@sae.org

ISBN 0-7680-1319-4
Copyright © 2004 SAE International

Positions and opinions advanced in this paper are those of the author(s) and not necessarily those of SAE. The author is solely responsible for the content of the paper. A process is available by which discussions will be printed with the paper if it is published in SAE Transactions.

Persons wishing to submit papers to be considered for presentation or publication by SAE should send the manuscript or a 300 word abstract of a proposed manuscript to: Secretary, Engineering Meetings Board, SAE.

Printed in USA

Vehicle Dynamics in Non-Collinear Low-Velocity, Rear End Collisions

Herbert M. Guzman and Whitman E. McConnell
Biodynamic Research Corporation

Darrin A. Smith
Injury Sciences Corporation

Copyright © 2004 SAE International

ABSTRACT

The vehicle dynamics of non-collinear, low-velocity front-to-rear collisions have received little formal study. The twenty-three angled collisions conducted for this project revealed significant vehicle dynamic differences when compared with similar-energy collinear rear-end collisions. Two recent model year vehicles were used to conduct non-collinear collisions at a nominal 12 km/h impact velocity. The pre-collision angles between the test vehicles were established so that the striking vehicle's line of action through its CG was either 15 or 30 degrees from the stationary struck vehicle's initial heading. Both vehicles had accelerometers at their CG's measuring longitudinal and lateral accelerations. The struck vehicle also had sensors to measure CG vertical accelerations, yaw rates, and longitudinal and lateral velocities. Film from three high-speed 16-mm [film] cameras was digitized and analyzed for each collision. The ΔV at various points within the struck vehicle was studied. The time-history of the center of rotation of the struck vehicle was analyzed and correlated to tire slippage. The ΔV of the struck vehicle decreased as the angle between vehicles increased from 15 to 30 degrees with energy dissipated by suspension motion and scrubbing of the struck vehicle's tires. For the struck vehicle, collisions at 15-degree angles were more akin to pure collinear rear-end collisions; collisions at 30-degree angles showed a more pronounced curvilinear-translation of the CG of the struck vehicle with rotation about a point near its left-front tire. Variations in translational and rotational vehicle dynamics with respect to impact angle were sufficient to alter the resulting occupant motion.

INTRODUCTION

The dynamics of vehicles in low-velocity rear-end collisions have been studied by many since the late 1950's and in more detail in the 1990's [1, 2, 3, 4, and 5]. However, all these studies have been with the striking and struck vehicles aligned *collinearly* and with

no lateral offset. The objective of this document is to describe the dynamics of non-collinear low-speed rear-end collisions. For this study, the striking vehicle's orientation was chosen at two specific angles with respect to the struck vehicle. Many non-collinear vehicle alignments are possible for these two angles, so a specific line of action was also chosen for each. The scope of this document does not include the detailed analysis of the struck vehicle occupant kinematics. These aspects are discussed in another document. [6]

METHODS

TESTING PROTOCOL

The testing consisted of a series of low-velocity front-to-rear collisions between a striking vehicle traveling at a nominal impact speed of 12 Km/h and a stationary vehicle (in neutral with brakes off). A ramp and earth's gravity were used to accelerate the striking vehicle into the target vehicle. The pre-collision angles between the test vehicles were established so that the striking vehicle's heading and velocity were either 15 or 30 degrees from the stationary struck vehicle's initial heading. Figure 1 shows the two test configurations with the chosen line of action for each. The striking vehicle was a 1996 Buick Skylark (1,644 kg) and the struck vehicle was a 1996 Ford Taurus (1,592 kg). The weight of the vehicles as tested and the location of their CG in the longitudinal and lateral directions were obtained by weighing the vehicles with separate scales under each wheel. The contacting surfaces of the vehicles were inspected and repaired throughout the test series. A portion of the inside tread of the left [driver] side tires and the outside tread of the right side tires was lightly painted with chalk to record the tire paths of the struck vehicle after each impact. Five male human subjects and one Hybrid III 50th percentile male Anthropomorphic Test Device (ATD) were used as occupants of the struck vehicle. The striking vehicle was unmanned and equipped with remotely controlled braking. Twenty-three tests were performed with various occupant positions.

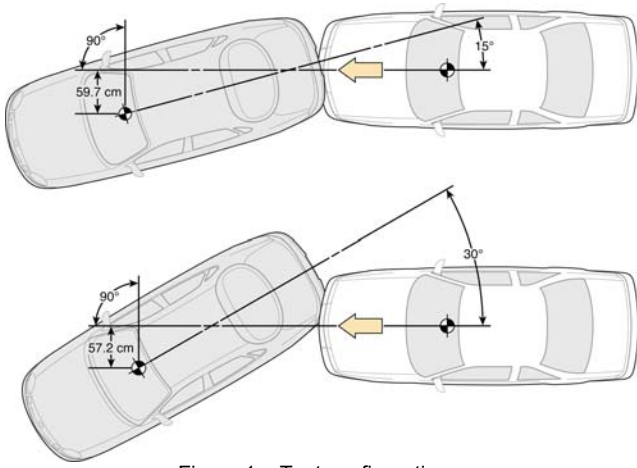


Figure 1 – Test configurations.

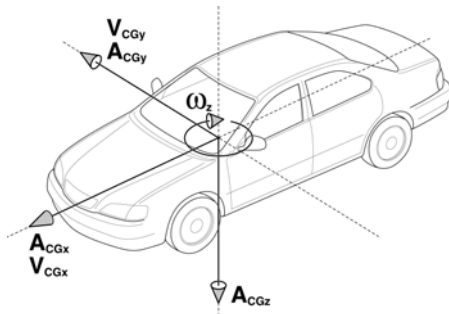


Figure 2 - Struck vehicle instrumentation.

digitization/3D-motion analysis software system could be used to track these markers [7]. The markers on the struck vehicle were selected primarily to obtain a time-history of the position of the vehicle's CG and its tires (Fig. 4).

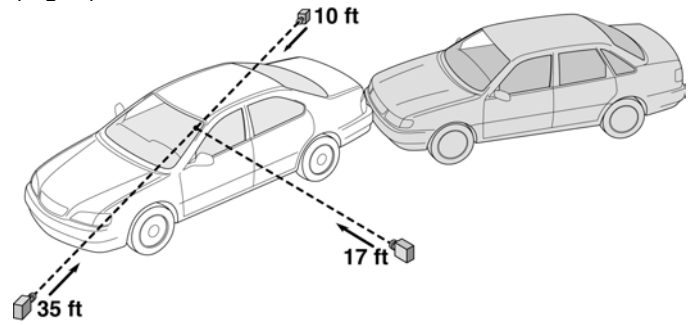


Figure 3 - Basic camera layout.

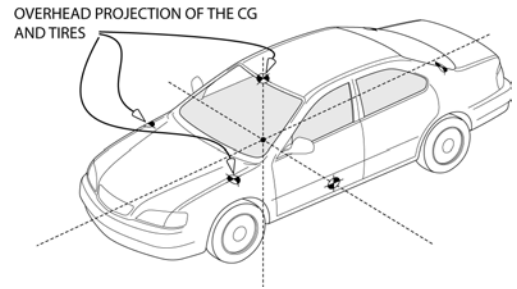


Figure 4 - Vehicle Markers.

ELECTRONIC INSTRUMENTATION

Both vehicles were instrumented with translational, gas-damped accelerometers at their CG's measuring longitudinal (A_{CGx}) and lateral (A_{CGy}) accelerations. The struck vehicle also had a translational accelerometer at its CG to measure vertical accelerations (A_{CGz}), a yaw rate (ω_z) sensor and two infra-red (IR) speed traps to measure longitudinal (V_{CGx}) and lateral (V_{CGy}) speeds at its CG (Fig. 2).

PHOTOGRAPHIC INSTRUMENTATION

Photographic data from the tests were recorded with three high-speed 16-mm motion picture cameras operating at nominally 500 frames/sec. The cameras were positioned to view the front, side and rear of the struck vehicle to obtain a three-dimensional visual description of the motion of the struck vehicle occupants (Fig. 3). For two tests, two of the 16-mm film cameras were used to record [at 500 frames/sec] the tires of the struck vehicle in 15° and 30° impact configurations. For one 30° test, the high-speed film cameras were used to record an overhead view of the struck vehicle. Overhead views of the impact zone of several 15° and 30° tests were also recorded with digital video at 30 frames/sec. The 16-mm film was transferred frame-by-frame to digital video files. The vehicle, human subjects and ATD were marked so that a computerized image

SYNCHRONIZATION OF ELECTRONIC AND PHOTOGRAPHIC INSTRUMENTATION

The timing of the sensor and film data was synchronized with a strobe visible from all three cameras. The strobe was triggered by a tape-switch on the initial contact point of the rear bumper of the struck vehicle. Simultaneously, when the strobe was triggered, a pulse was recorded by the data acquisition system.

ELECTRONIC SENSOR DATA PROCESSING

All electronic sensor signals were recorded using a 12-bit data-acquisition system sampling at 10,000 Hz per channel. The signals were pre-filtered with an analog 4-pole, low-pass Butterworth filter with a nominal cutoff frequency of 1650 Hz (SAE J211-1, CFC1000) [8].

Vehicle Accelerations

The Power Spectral Densities (PSD's) for the vehicle accelerations were obtained. The PSD, S_X of a signal $X(t)$, is defined as:

$$S_X(f) = \int_{-\infty}^{\infty} R_X(\tau) e^{-j2\pi f\tau} d\tau, \quad (1)$$

where R_x is the autocorrelation function of the signal [9]. The PSD's for the acceleration components revealed that most of the power in the frequency spectra was concentrated in frequencies below 500 Hz. Figures 5(a) and 5(b) show typical PSD's obtained for the struck vehicle [sensor] acceleration signals.

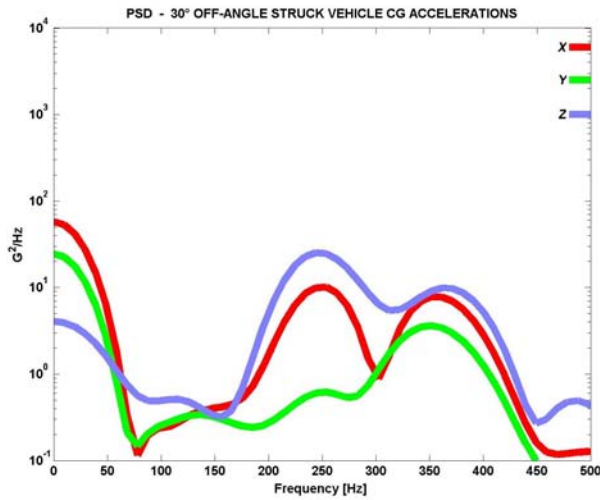


Fig. 5(a) – PSD for Struck Vehicle CG Accelerations (30°).

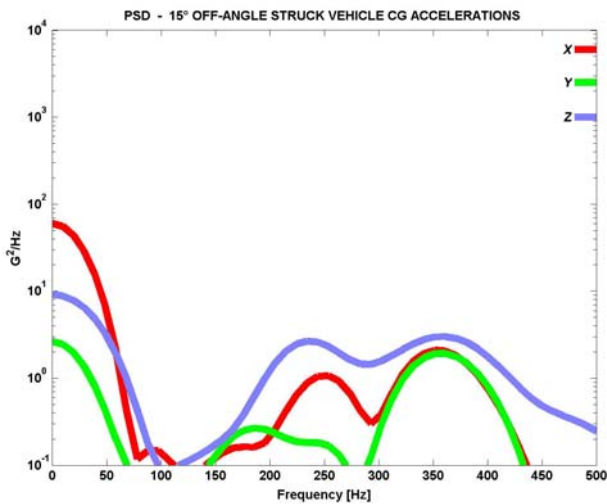


Fig. 5(b) - PSD for Struck Vehicle CG Accelerations (15°).

Prior to integrating into velocity and displacement, the vehicle accelerations were filtered with a CFC180 [8] digital, low-pass Butterworth filter with an upper cutoff of 300-Hz. The additional filtering reduced the higher frequency vibrations but did not attenuate the overall acceleration pulse. The CFC180-filtered signals were compared with the original signals to verify the data were not attenuated significantly. Figures 6(a) & (b) show typical vehicle accelerations comparing filtered versus original signals for 30° and 15° tests. The

velocities and displacements were then computed for comparison with film-derived signals.

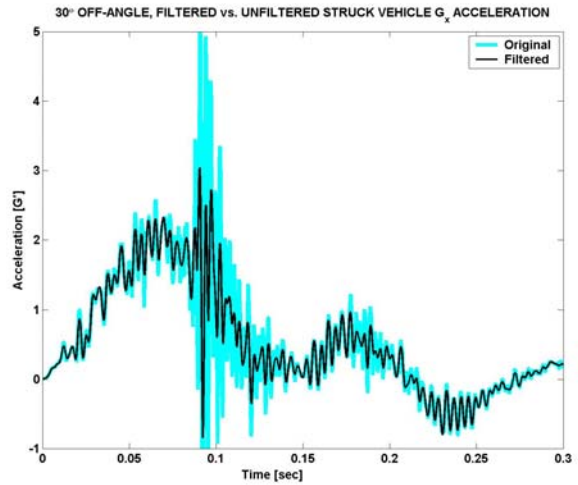


Fig. 6(a) – Typical Raw vs. Filtered Vehicle Acceleration Signal (30°).

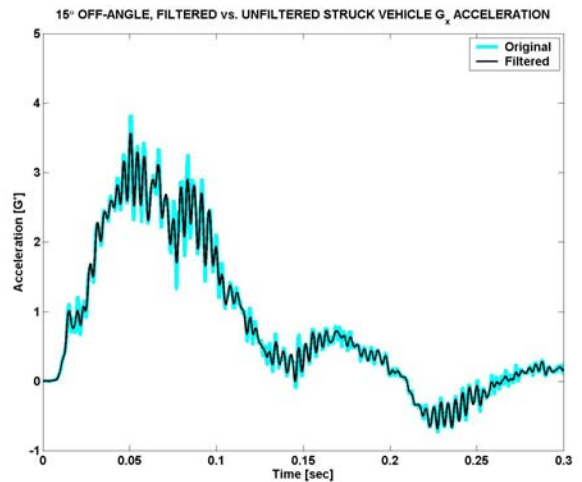


Fig. 6(b) – Typical Raw vs. Filtered Vehicle Acceleration Signal (15°).

Rotational Rates

The PSD's for the vehicle yaw [rotational] rates were also obtained to determine if additional smoothing/filtering was appropriate using a method similar to that used to process the translational acceleration signals. Figure 7 shows typical PSD's for yaw rates for 30 and 15 degree tests. To reduce higher frequency vibrations, the yaw rates were filtered with a CFC60 digital filter [8]. The yaw rates were then integrated and differentiated into rotational displacements and accelerations, respectively.

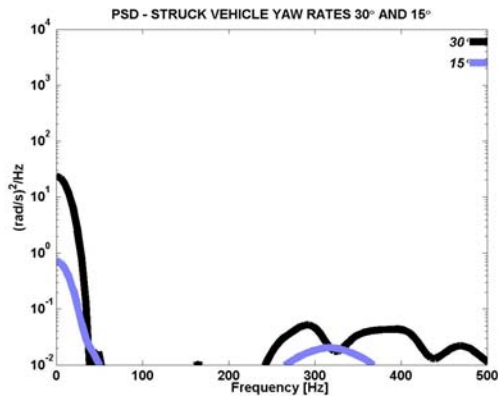


Figure 7 – Typical PSDs for 30° and 15° Tests.

RESULTS

Twenty-three non-collinear tests were performed, 11 were at 15° and 12 at 30°. In addition, one test was performed with a 20° configuration and one in a collinear alignment. For all tests, the closing speed of the striking vehicle ranged from 11.8 to 12.4 km/h with the corresponding impact energies of 8778 to 9663 N-m.

The dynamics of the struck vehicle upon impact, in both the 15° and 30° configurations showed an initial period of yaw more so for the 30° configurations; the striking vehicle essentially continued its motion in a straight path. The yawing of the struck vehicle produced a different ΔV at different locations within this vehicle. The ΔV of the struck vehicle measured at its CG ranged from 5.9 to 7.1 km/h for the 30° tests, while the ΔV ranged from 9.0 to 9.4 km/h for the 15° tests. The restitution coefficient for the 30° tests was between 0 and 0.20 while for the 15 degree tests it was between 0.47 and 0.53. The peak yaw rate for the 30° tests ranged from 0.57 to 0.60 rad/s; the peak yaw rate for the 15° tests ranged from 0.18 to 0.20 rad/s. The details of the 20° test are included in the appendix (Fig. A1). The struck vehicle ΔV for the collinear test was 9.1 km/h and the restitution coefficient was 0.49. Table A1 in the appendix section includes a summary of the results for all the tests.

The vehicles were inspected prior to and subsequent to each test and the bumper assemblies including absorbers were replaced if damage was noted. In all, there was little cumulative damage to the struck vehicle, but the front end of the striking vehicle progressively accumulated minor damage, despite recurrent interval repairs. During the last 30° test, the [damaged] left-front of the striking vehicle “hooked” the left-rear bumper edge of the struck vehicle producing slightly more yaw than seen in the previous 30° runs.

The coefficient of friction of the struck vehicle tires on the testing surface was measured by dragging the whole vehicle at the tested 15 & 30 degree angles. This was repeated several times during and after the test series; the coefficient of friction of the system remained nominally at 0.6 throughout.

COLLISIONS AT 30-DEGREES

In this test configuration, the rear tires of the struck vehicle lost lateral traction side-slipping a total of 10 to 22 inches rightward as the vehicle moved forward. The front tires did not sideslip, but the chalk tracks indicated that the whole vehicle rotated around a point located near the left-front tire. Figure 9 shows typical [CG] longitudinal and lateral accelerations and speeds for a 30° test.

FILM DATA PROCESSING

The 16-mm film cameras recorded each of the events at a nominal rate of 500 frames/sec. A 3D calibration frame with markers spaced at known distances was included in the footage at the end of each test. The footage of this calibrator was included in the digital [AVI] files produced from each test. The calibrator allowed the motion analysis software to scale and track, frame-by-frame the 3D position of the vehicle and occupant's markers in each test. At a glance, the raw position-time data appeared smooth, but when numerically double-differentiated, the resulting accelerations were extremely noisy. The PSD's for the digitized position-time data revealed that most of the power in the frequency spectra was concentrated in frequencies below 20-30 Hz. Figure 8 shows typical PSD's observed for the vehicle CG (x) position-time signals from the digitized film. The digitized film *position* data were filtered with a 20-Hz upper cutoff, low-pass Butterworth filter. The results of the vehicle accelerations derived from the digitized film and those measured with the accelerometers are compared in the discussion section. Further details of the processing and validation of the film data from this test series are discussed in a separate document [10].

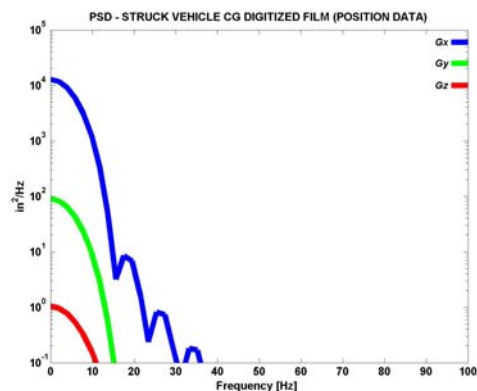
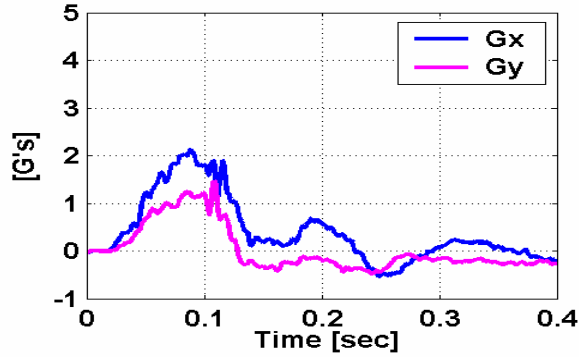


Fig. 8 – Typical PSDs for Vehicle Displacements (from Film).

LONGITUDINAL & LATERAL ACCELERATIONS



LONGITUDINAL & LATERAL SPEEDS

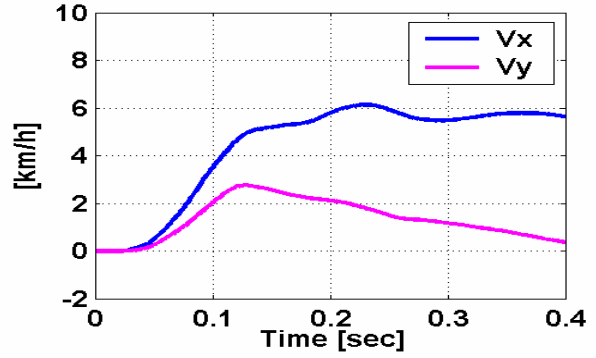
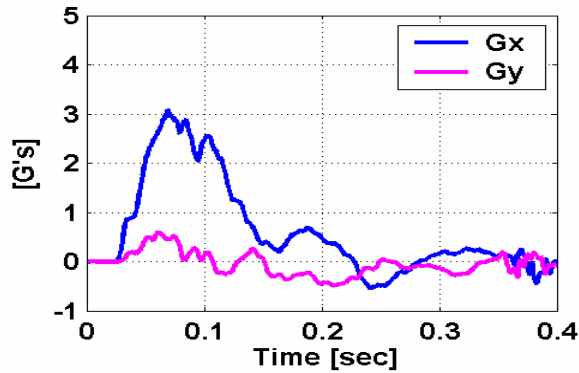


Figure 9 – Struck Vehicle CG Translational Speeds and Accelerations (30°).

LONGITUDINAL & LATERAL ACCELERATIONS



LONGITUDINAL & LATERAL SPEEDS

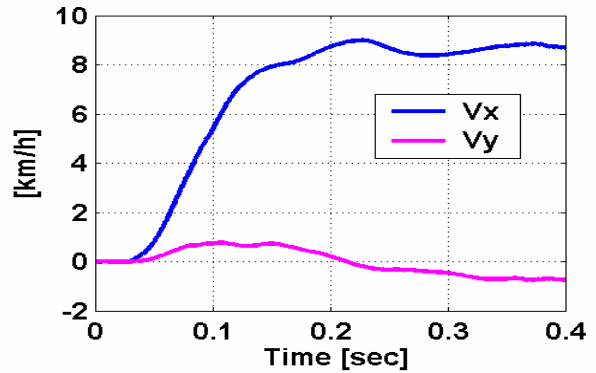
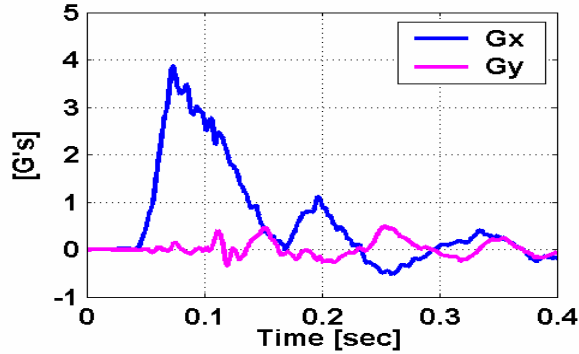


Figure 10 – Struck Vehicle CG Translational Speeds and Accelerations (15°).

LONGITUDINAL & LATERAL ACCELERATIONS



LONGITUDINAL & LATERAL SPEEDS

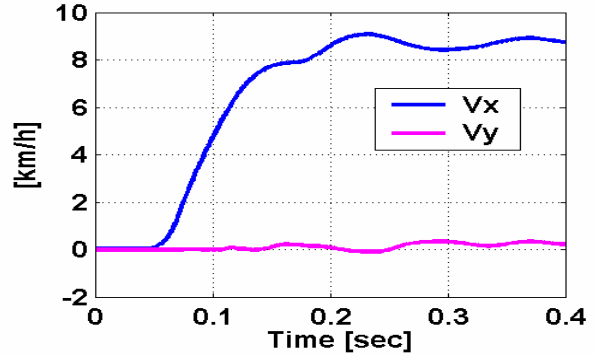


Figure 11 – Struck Vehicle CG Translational Speeds and Accelerations (0°).

COLLISIONS AT 15-DEGREES

In the 15° tests, the rear of the car moved rightward but did not slip sideways. Only the suspension was noted to “heave” rightward during the early impact period. The result was that the rear body of the vehicle yawed rightward perceptibly while the final vehicle trajectory did

not change from its original 15° heading. Figure 10 shows typical [CG] longitudinal and lateral accelerations and speeds for a 15° test. For comparison, the [CG] longitudinal and lateral accelerations and speeds of the collinear (i.e. 0°) test performed with the same vehicles is shown in figure 11. Also, Figure 12 shows a comparison of typical yaw rates for 15° and 30° tests.

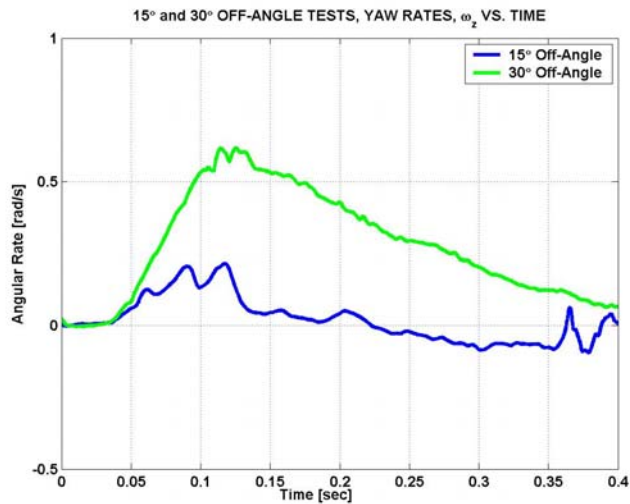


Figure 12 – Typical yaw rates for 15° and 30° tests.

DISCUSSION

Comparing the 15° and 30° tests, it was noted that as the angle of the struck vehicle off the striking vehicle's direction increased, the overall ΔV of the struck vehicle decreased despite the similar input energies. This is evident in the magnitude of the CG acceleration pulses of figures 9 and 10 above. Furthermore, the [CG] longitudinal acceleration pulses for the 30°, 15° and 0° collisions were characterized by a bimodal waveform with an initial pulse approximately 130-150-ms long followed by a second lower magnitude pulse approximately 70-80-ms long. The second peak in these waveforms appears to be associated with the slight override of the striking vehicle's bumper over the bumper of the struck vehicle. The [CG] lateral acceleration pulses were typically lower in magnitude for the 15° and 0° tests than the magnitude of the pulses in the 30° tests.

In the 30° tests, the rear end of the struck vehicle slewed rightward, scrubbing the rear tire treads across the pavement. In effect, a portion of the struck vehicle's kinetic energy was in the form of rotational energy rather than translational energy. Therefore, the translational velocity change was lower. Figure 13 shows a right rear tire mark from a 30 degree test. (The terminal perturbation is from a late second strike by the Buick).

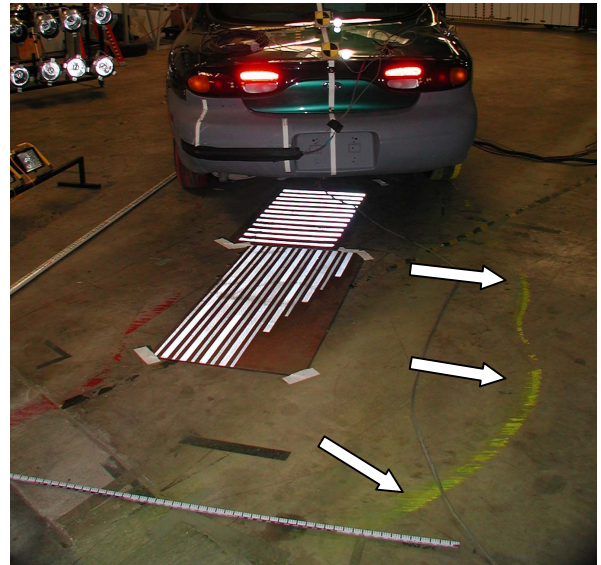


Figure 13 – 30° test, right-rear tire track (Arrows).

Figure 14 shows the darker track of the yawing right [front] wheel as the direction of the vehicle changed during impact. Average yaw was approximately 6 to 10 degrees for the 30 degree test series. Figure 15 shows the final position of the struck vehicle after a 30 degree test. The total angle shown in figure 15 was measured to be approximately 8-9 degrees.



Figure 14 – 30° test, right-front tire track (Arrows).

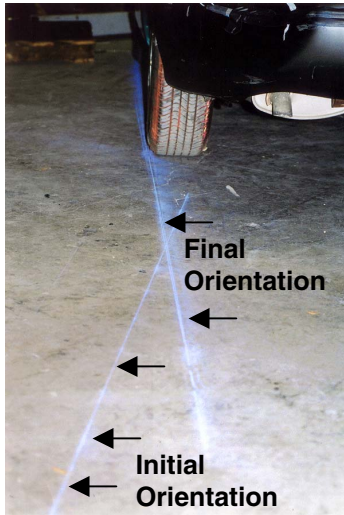


Figure 15 – Approximate total rotation of struck vehicle (30° Test).

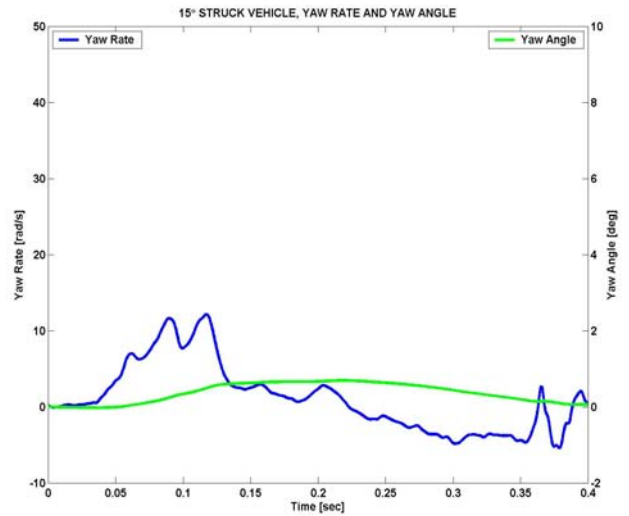


Figure 16(b) – Typical yaw rate and yaw angle for 15° test.

The amount of rotation as determined by integration of the yaw rate sensor data was in the range of 6.5 degrees for the 30° tests. In the 15° tests, the struck vehicle only rocked on its suspension. Figures 16(a) and 16(b) show the yaw rate and the yaw rotation versus time for the struck vehicle in the 30° and 15° tests, respectively.

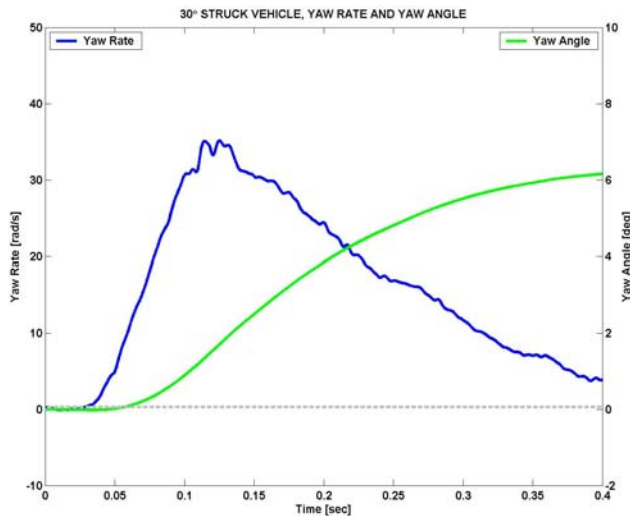


Figure 16(a) – Typical yaw rate and yaw angle for 30° test.

INSTANTANEOUS CENTER OF ROTATION OF THE STRUCK VEHICLE

Analysis of the high-speed photography of the struck vehicle's tires indicated that in the 30° tests, the vehicle initially rotated (yawed) about a translating point on the ground under or near the left-front tire. An overhead view of the struck vehicle's motion showed that the left-front tire essentially traveled in a straight line while the rear of the vehicle yawed to the right. However, in the 15° tests, the struck vehicle essentially rocked on its suspension while rolling forward. Based on this, the estimation of the instantaneous center of rotation of the struck vehicle was focused on the 30° tests as follows. First, the motion of the struck vehicle was divided into three phases: Phase 1, from first contact to approximately 40 ms involved compression of the vehicles' bumpers. Phase 2, from approximately 40 to 130 ms involved pronounced rotation of the struck vehicle; and Phase 3 from approximately 130 to about 340 ms involved continuing rotation combined with significant translation forward. After approximately 300-340 ms, the vehicles began to separate and the struck vehicle translated forward to a stop with no appreciable rotation. Figures 17(a)-(c) show the struck vehicle's phases for the 30° tests. In Phase1, there was no observable vehicle motion; the predominant rotation in phase 2, allowed estimation of the instantaneous center of rotation during this phase.

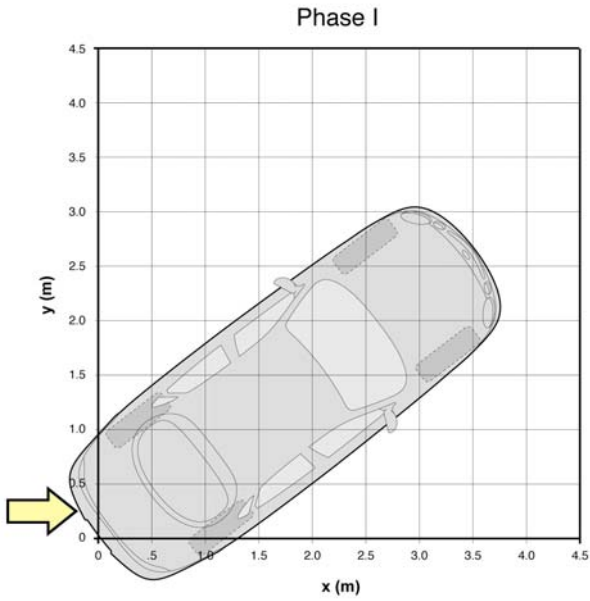


Fig. 17(a) – Phase 1, bumper compression (approx. 40 ms).

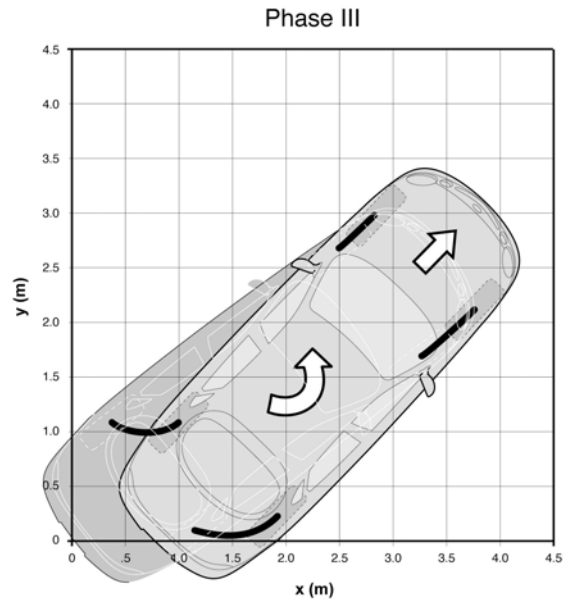


Fig. 17(c) – Phase 3, rotation and translation (approx. 130-340 ms).

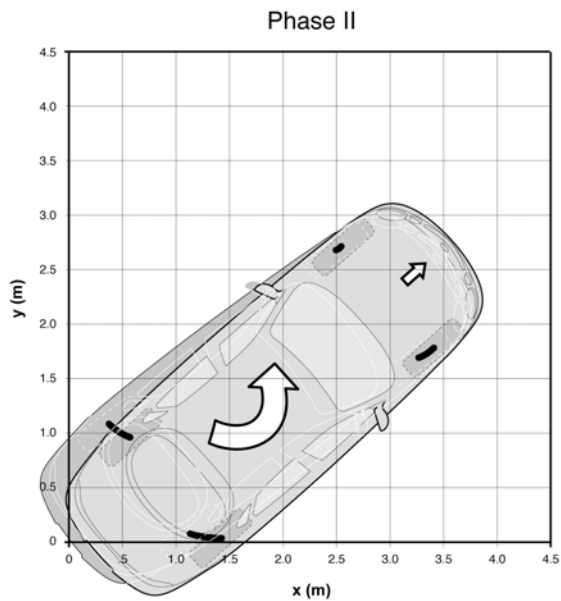


Fig. 17(b) – Phase 2, pronounced rotation (approx. 40-130 ms).

Phase 2

During this phase, the yaw rate and the CG's lateral ΔV reached their peaks and the vehicle's rotation was mostly about an area under its left-front tire. The predominant rotation of the vehicle was evident when comparing the digitized displacement of the left-side tires. The displacement with the steepest slope (i.e. highest rate) and greatest magnitude was the left-rear tire's lateral displacement. The left-front tire's forward displacement was the lowest. Figure 18 compares these displacements and figures 19(a) & (b) show the vehicle's typical rotational and translational rates and accelerations for this phase.

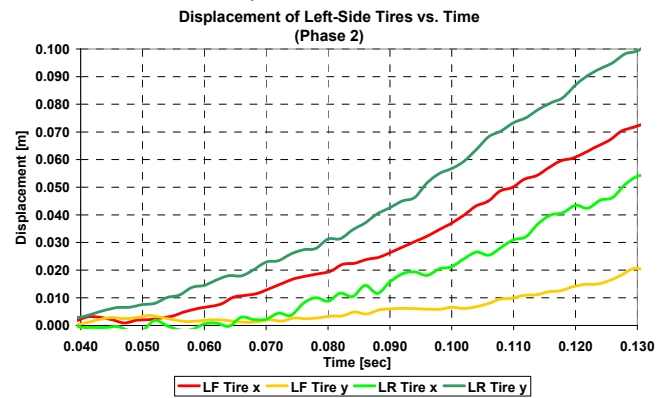


Figure 18 – Digitized displacement of vehicle's left-side tires (phase 2).

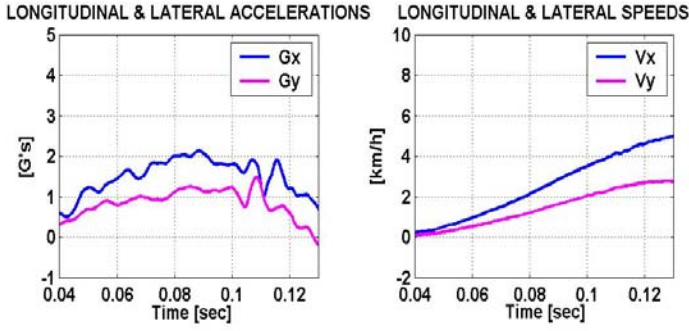


Figure 19(a) – Translational accelerations and velocities for phase 2.

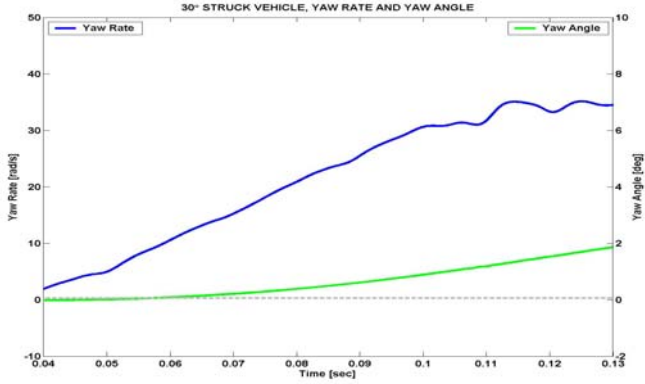


Figure 19(b) – Rotational [yaw] velocity and displacement for phase 2.

The acceleration at the vehicle's CG (\vec{A}_{CG}) was defined as the acceleration of the left-front tire (\vec{A}_{LFTire}) plus the acceleration at the CG with respect to the left-front tire ($\vec{A}_{CG/LFTire}$) or:

$$\vec{A}_{CG} = \vec{A}_{LFTire} + \vec{A}_{CG/LFTire} \quad (2)$$

$$\vec{A}_{CG} = \vec{A}_{LFTire} + \vec{\omega} \times (\vec{\omega} \times \vec{R}) + \vec{\alpha} \times \vec{R} \quad (3)$$

The acceleration of the left-front tire was much lower than that of the CG during this phase; therefore, \vec{A}_{LFTire} does not contribute significantly to equation (3) and the acceleration of the CG with respect to the ground becomes:

$$\vec{A}_{CG} = \vec{\omega}^2 \times \vec{R} + \vec{\alpha} \times \vec{R} \quad (3B)$$

Therefore, the magnitude of the tangential and radial accelerations of the vehicle's CG can be written as:

$$A_n = \omega^2 R, \quad (4)$$

and

$$A_t = \alpha R, \quad (5)$$

The yaw [rotational] acceleration, α was determined by numerical differentiation of the measured yaw rate and R was the distance to the instantaneous center of rotation. As shown later, a mean distance for R (during phase 2) was calculated to be 90 inches. Figure 20 illustrates

these components and the typical rotational components calculated for a 30° test are shown in figure 21.

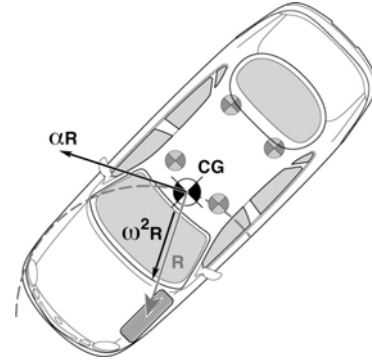


Figure 20 – Phase 2, CG resultant acceleration, resolved into rotational components.

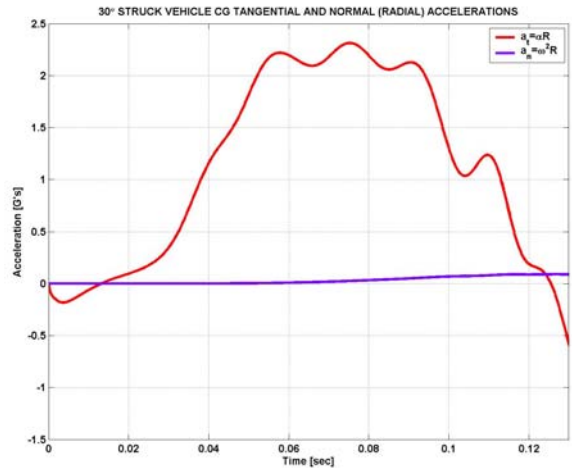


Figure 21 – Phase 2, tangential and normal accelerations.

From figure 21, it can be observed that for this phase, the radial/normal acceleration component A_n is small compared to the tangential acceleration A_t , that is:

If $A_n \ll A_t$, then:

$$A_t \cong \sqrt{A_{CGx}^2 + A_{CGy}^2} = \|\vec{A}\| = A_{result} \quad (6)$$

$$A_t = \alpha R \cong A_{result} \quad (7)$$

where, A_{cgx} and A_{cgy} are the accelerations of the struck vehicle's CG as measured by the translational accelerometers; A_{result} is the struck vehicle's CG resultant acceleration; and R is the distance from the instantaneous center of rotation to the vehicle's CG. An estimate of the time-history of R for this phase can be

obtained by the following approximation based on equation (7):

$$R(t) \cong \frac{\sqrt{A^2_{CGx} + A^2_{CGy}}}{\alpha} \quad (8)$$

Figure 22(a) shows an example of an estimate of the radius of rotation (R) of the struck vehicle's CG while the vehicle sustained pronounced yaw. The distance from the center of the left-front tire on the struck vehicle to the vehicle's estimated CG [in the yaw plane] was measured to be 60 inches. The mean radius estimated using equation (8) (phase 2 only) was 90±5 inches based on data from the 30° tests. A comparison of the resultant acceleration of the struck vehicle CG calculated from the translational accelerometer signals (A_{CGx} and A_{CGy}) and the resultant acceleration using equations (4) and (5) with a constant R of 95 inches [as an example] is shown in Figure 22(b).

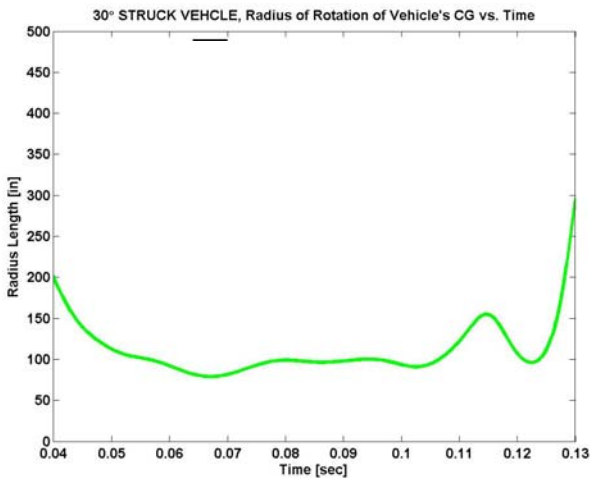


Fig. 22(a) – Estimate of radius of rotation.

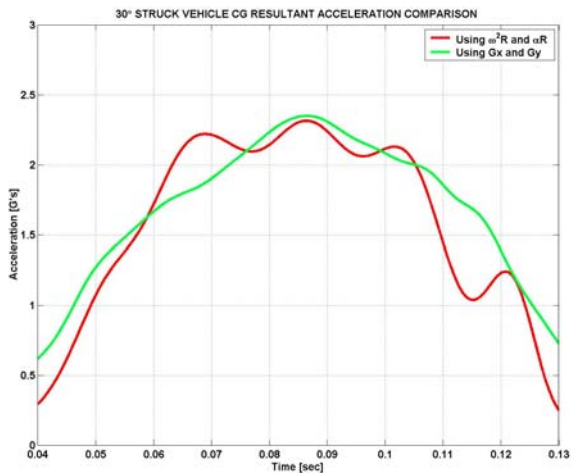


Fig. 22(b) – Struck vehicle CG resultant accelerations.

For this phase, the resultant accelerations at various regions of the vehicle can be estimated (in the yaw plane) using the tangential and normal acceleration components (Eqns. 4 and 5), and the measured yaw rate and acceleration. Figure 23 is an example of several estimates.

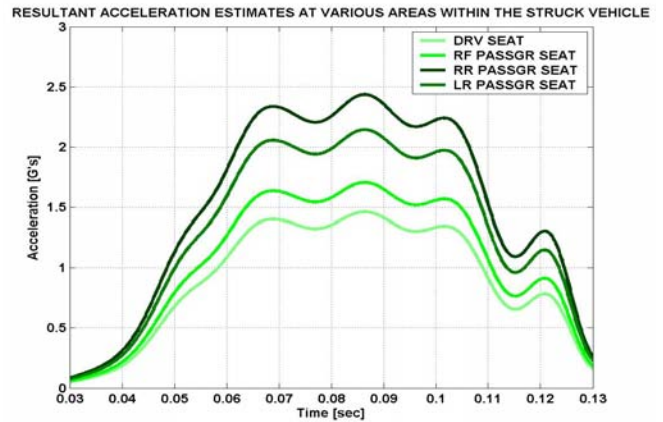


Figure 23 – Phase 2, resultant accelerations at various points in the vehicle.

Phase 3

During this phase, the vehicle still rotated about an area near the left-front tire but also experienced significant forward translation. This was observed in the digitized displacement of the left-side tires during this phase (figure 24). The left-front tire traveled in a straight line while the left-rear tire traveled forward and to the right. For this phase, the slope (i.e. rate) of the forward displacement of the left-front tire was the steepest. Based on this, the speed and acceleration of the vehicle's left-front tire would be considerably higher than in phase 2 and the instantaneous center of rotation for the vehicle could not be estimated as in phase 2.

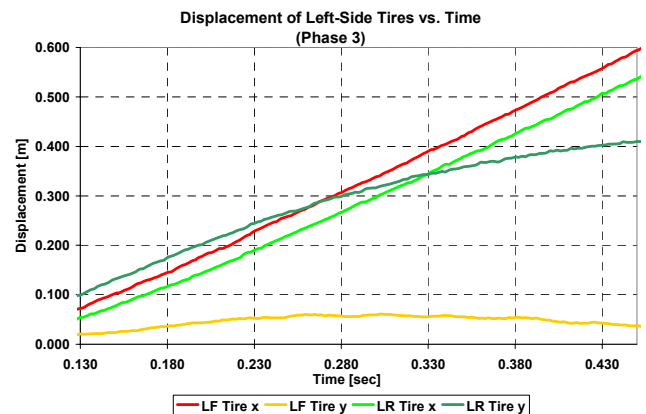


Figure 24 – Digitized displacement of vehicle's left-side tires (phase 3).

Nevertheless, the vehicle's acceleration measured at its CG decreased and its yaw rate and CG's lateral ΔV decreased while the CG's forward ΔV reached its peak. Figures 25(a) & (b) show the typical rotational and translational rates and accelerations for this phase.

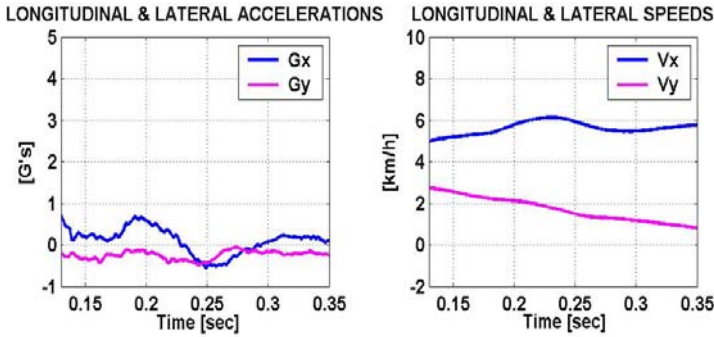


Figure 25(a) – Translational accelerations and velocities for phase 3.

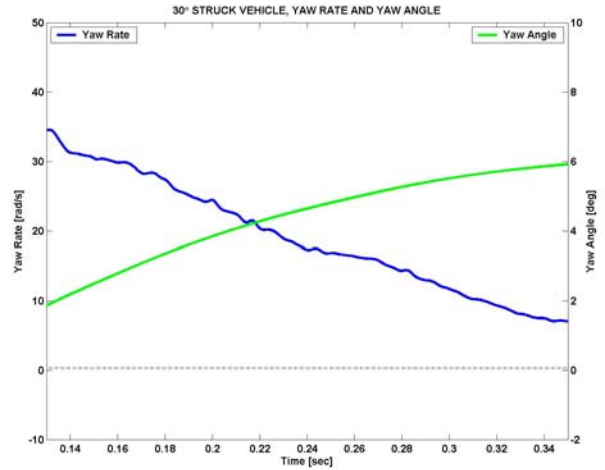


Figure 25(b) – Rotational [yaw] velocity and displacement for phase 3.

HIGH-SPEED FILM DATA VS SENSOR DATA

The digitized displacement of the struck vehicle's CG in the longitudinal and lateral directions was numerically differentiated and compared with the accelerometer signals and with the integrated accelerometer signals. The film data showed good correlation with the accelerometer data (see Figures 26(a) and 26(b)).

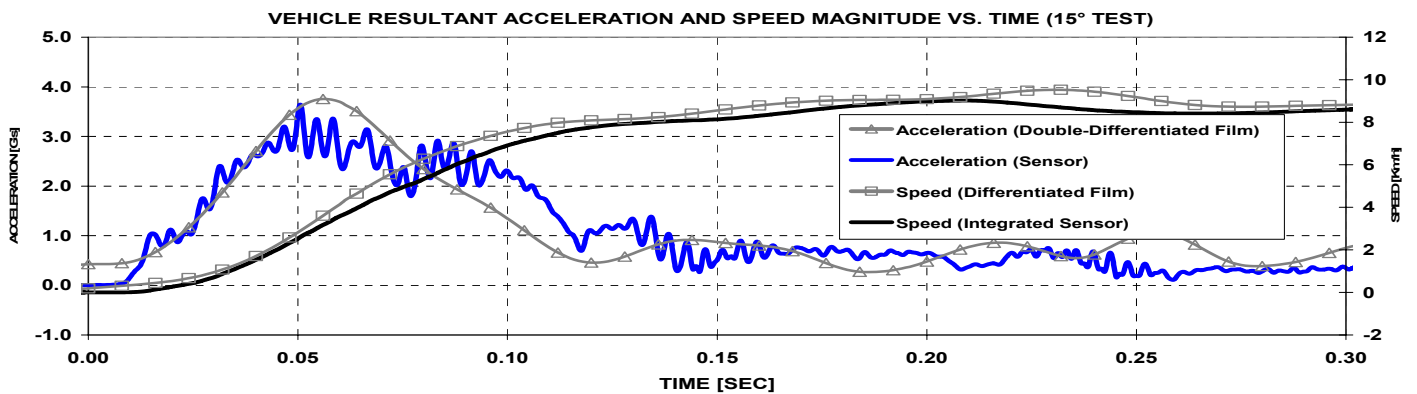


Figure 26(a) – Comparison of film vs. sensor data (15° Test).

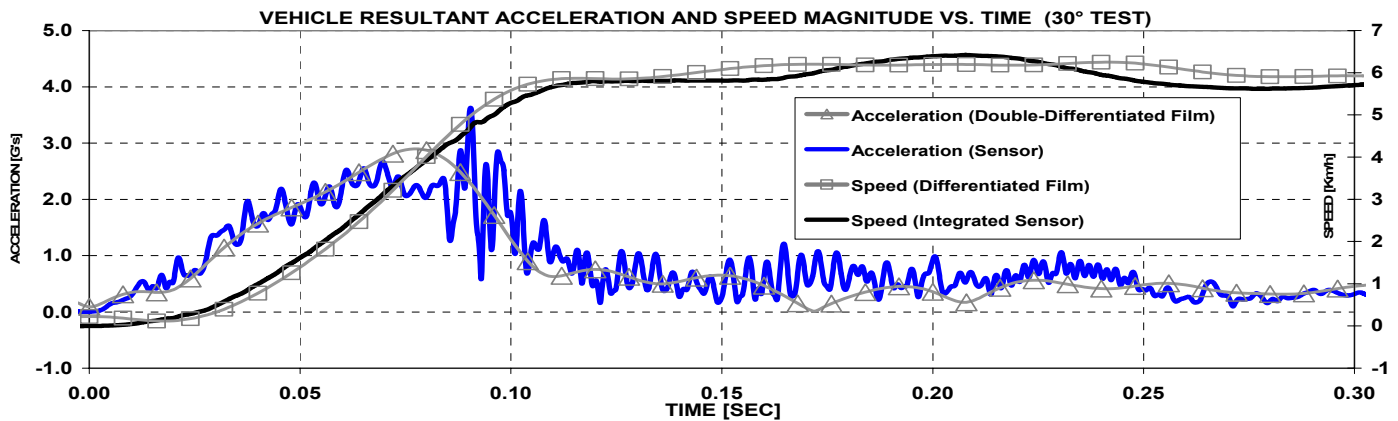


Figure 26(b) – Comparison of film vs. sensor data (30°).

CONCLUSION

The primary objective of this document was to describe the dynamics of low-velocity front-to-rear, non-collinear collisions. The scope of this document was on 15° and 30° angles between the heading and velocity of the striking vehicle and the struck vehicle's initial heading for a specific line of action in each case. The closing speed of the striking vehicle was maintained at nominally 12 km/h. The tests performed in this project revealed that 15° low-velocity front-to-rear collisions were more akin to collinear collisions. The ΔV of the struck vehicle in the 15° tests was similar to that of the struck vehicle in a purely collinear front-to-rear test with equivalent input energy. The coefficient of restitution in the 15° tests was nearly the same as that of a collinear collision with equivalent input energy. Low-velocity collisions at 30° were characterized by three phases; approximately 40-ms of initial bumper compression followed by about 30 ms of pronounced yaw with minimal translation. The third phase, which was approximately 300-ms long, involved continued rotation combined with significant forward translation. For the second phase, an instantaneous radius of rotation was estimated, and the accelerations at various points in the vehicle were estimated. In both the 15° and 30° tests, the striking vehicle continued traveling with its pre-impact orientation. Lastly, the restitution coefficient for the 30° tests approached zero.

ACKNOWLEDGMENTS

Special thanks to the Biodynamic Research Corporation, Research Test Center staff: Roy Meredith, John Kush, Darrell Bay and Enrique Bonugli. Also thanks to the Visual Communications department staff: Bob Carlin and Robert Reyes.

REFERENCES

1. Severy, D. M. et al. "Controlled Automobile Rear-End Collisions, An Investigation of Related Engineering and Medical Phenomena." *Canadian Services Medical Journal*, 1955, vii, pp. 727-59.
2. McConnell, W. et al. "Analysis Of Human Test Subject Kinematic Responses to Low Velocity Rear End Impacts." *1993 International SAE Congress and Exposition*, Detroit, 1993.
3. McConnell, W. et al. "Human Head and Neck Kinematics After Low-Velocity Rear-End Impacts." *39th Stapp Car Crash Conference*, San Diego, CA, 1995.
4. Siegmund, G. P.; Bailey, M. N.; King, D. J. (1994) Characteristics of specific automobile bumpers in low-velocity impacts. IN: *Accident Reconstruction: Technology and Animation IV (SP-1030)*. Warrendale, PA, Society of Automotive Engineers, 1994, pp. 333-372 (SAE Paper #940916).
5. Szabo, T.J.; Welcher, J. (1992) Dynamics of low speed crash tests with energy absorbing bumpers. IN: *Automobile Safety: Present and Future Technology (Society of Automotive Engineers SP-925)*. Warrendale, PA, Society of Automotive Engineers, 1992, pp. 1-9 (SAE Paper #921573).
6. McConnell, W. E., et al. "Non-Collinear Low Velocity Rear End Collision Human Kinematics." *The Association for the Advancement of Automotive Medicine*, Lisbon, Portugal, 2003.
7. User's manual, *WINalyze Automatic Motion Analysis V. 1.4*; Mikromak, 1998.

8. SAE J211-1 Instrumentation for Impact Test – Part 1 – Electronic Instrumentation, 2003 SAE Handbook, Warrendale, PA, Mar. 1995
9. Haykin, Simon, Communication Systems, New York: John Wiley & Sons, Inc., 1994.
10. Guzman, H.M., et al. “Human Acceleration Measurements in Low-Speed, Angled Rear End Collisions.” Instrumentation Systems, and Automation Society, EXPO 2003, Houston, Texas, 2003.

APPENDIX

Table A1 summarizes the test results including the 20° and the collinear test results. Figure A1 shows the accelerations and speeds of the struck vehicle in the 20° test. The struck vehicle ΔV for the 20° test was 8.7 km/h and the restitution coefficient was 0.43; the peak yaw rate for this latter test was 0.32 rad/s.

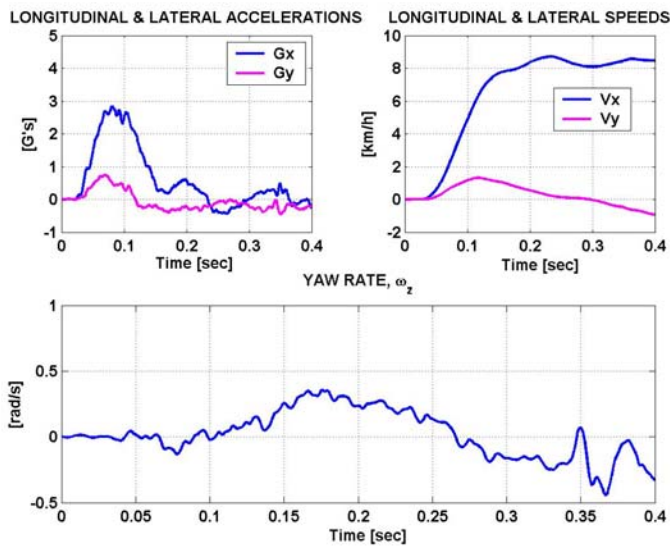


Figure A1 – Struck Vehicle CG Translational Speeds and Accelerations (20° Test).

TABLE A1. SUMMARY OF TEST RESULTS

#	Striking Vehicle						Struck Vehicle					Restitution Coefficient
	Closing Speed [mph]	Closing Speed [km/h]	Input Energy [lbs-ft]	Input Energy [N-m]	ΔV_{CG} [mph]	ΔV_{CG} [km/h]	Angle [°]	Resultant ΔV_{CG} [mph]	Resultant ΔV_{CG} [km/h]	Estimated G_x , Initial Pulse Width [ms]	Peak Yaw Rate [rad/s]	
1	7.4	12.0	6670	9044	5.4	8.7	15	5.6	9.0	137	0.20	0.48
2	7.5	12.1	6814	9240	5.5	8.8	15	5.6	9.0	135	0.18	0.47
3	7.4	11.9	6616	8971	5.5	8.9	15	5.8	9.3	150	0.19	0.53
4	7.5	12.1	6778	9191	3.9	6.2	30	4.0	6.4	135	0.60	0.05
5	7.5	12.0	6706	9093	3.9	6.3	30	4.1	6.5	128	0.58	0.07
6	7.4	11.8	6527	8850	4.0	6.5	30	4.1	6.6	131	0.57	0.11
7	7.5	12.0	6706	9093	4.0	6.4	30	4.1	6.6	140	0.58	0.09
8	7.4	11.8	6545	8874	4.2	6.8	30	4.4	7.1	-	-	0.17
9	7.4	11.9	6562	8899	5.5	8.8	15	5.7	9.1	136	-	0.51
10	7.7	12.4	7126	9663	5.6	9.1	15	5.8	9.4	170	-	0.49
11	7.4	12.0	6670	9044	5.6	9.0	15	5.8	9.3	173	-	0.53
12	7.3	11.8	6474	8778	3.9	6.3	30	4.1	6.6	128	-	0.09
13	7.5	12.1	6778	9191	3.9	6.2	30	4.0	6.4	150	-	0.04
14	7.5	12.1	6850	9289	3.9	6.2	30	4.0	6.4	120	-	0.04
15	7.5	12.0	6724	9117	3.6	5.7	30	3.7	5.9	135	-	0.00
16	7.5	12.1	6778	9191	3.8	6.1	30	3.9	6.3	135	-	0.03
17	7.4	11.9	6634	8995	5.4	8.6	15	5.6	9.0	135	-	0.48
18	7.4	11.9	6634	8995	5.4	8.8	15	5.6	9.0	146	-	0.49
19	7.3	11.8	6509	8826	5.5	8.9	15	5.7	9.1	135	-	0.52
20	7.4	11.9	6580	8923	5.5	8.8	15	5.7	9.2	150	-	0.52
21	7.5	12.1	6869	9314	5.6	8.9	15	5.7	9.2	140	-	0.49
22	7.4	11.9	6634	8995	3.6	5.7	30	3.7	6.0	150	-	0.00
23	7.6	12.2	6905	9363	3.7	6.0	30	3.9	6.2	128	-	0.00
A	7.4	12.0	6688	9068	5.2	8.4	20	5.4	8.7	140	0.32	0.43
B	7.5	12.0	6760	9166	2.0	3.2	0	5.6	9.1	126	-	0.49